Nguyen, T. H., Perillli, D., Cattelan, M., Liu, H., Sedona, F., Fox, N., Di Valentin, C., & Agnoli, S. (2019). Microscopic insight into the single step growth of in-plane heterostructures between graphene and hexagonal boron nitride. *Nano Research*, *12*(3), 675-682. https://doi.org/10.1007/s12274-019-2276-0

**Microscopic insight into the single step growth of in-plane heterostructures between graphene and hexagonal boron nitride**

Thanh Hai Nguyen,[1] Daniele Perilli,[2] Mattia Cattelan,[1,3] Hongsheng Liu[2] Francesco Sedona,[1] Neil A. Fox,[3] Cristiana Di Valentin,[2] Stefano Agnoli[1]*

*1 Department of Chemical Sciences University of Padova, Via Francesco Marzolo 1, 35131 Padova (Italy).*

*2 Dipartimento di Scienza dei Materiali, Università di Milano-Bicocca, via R. Cozzi 55, 20125 Milano, Italy*

*3 School of Chemistry, University of Bristol, Cantocks Close, Bristol BS8 1TS (UK)*

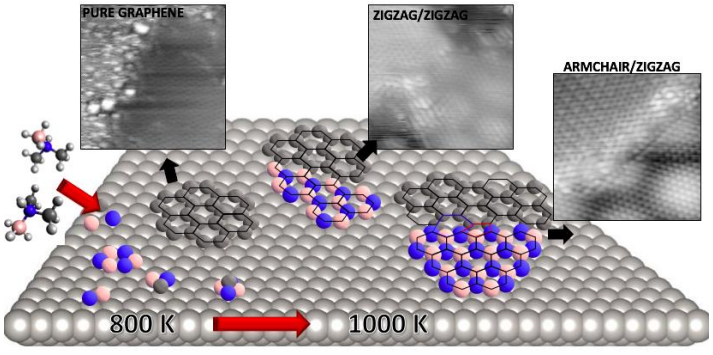


.

A variety of h-BN/graphene nanostructures can be obtained by the controlled decomposition of dimethylamino borane complex on the Pt(111) surface at different temperatures, which encompass B and N doped graphene layers, h-BN/Graphene 2D Janus quantum dots, and h-BN/graphene patchy layers. For the first time we report a quite unique 2D heterostructure where the graphene armchair edges are seamlessly connected to the h-BN zigzag edges.

Nano Research

ISSN 1998-0124 CN 11-5974/O4
https://doi.org/(automatically inserted by the publisher)



# Microscopic insight into the single step growth of in-plane heterostructures between graphene and hexagonal boron nitride

Thanh Hai Nguyen,[1] Daniele Perilli,[2] Mattia Cattelan,[1,3] Hongsheng Liu[2] Francesco Sedona,[1] Neil A. Fox,[3] Cristiana Di Valentin,[2] Stefano Agnoli[1](✉)

*1 Department of Chemical Science University of Padova, Via Francesco Marzolo 1, 35131 Padova (Italy).*
*2 Dipartimento di Scienza dei Materiali, Università di Milano-Bicocca, via R. Cozzi 55, 20125 Milano, Italy*
*3 School of Chemistry, University of Bristol, Cantocks Close, Bristol BS8 1TS (UK)*



**Received:** day month year / **Revised:** day month year / **Accepted:** day month year (automatically inserted by the publisher)

## ABSTRACT

Graphene-h-BN hybrid nanostructures are grown in one step on the Pt(111) surface by ultra-high vacuum chemical vapor deposition using a single precursor, the dimethylamino borane complex. By varying the deposition conditions, different nanostructures ranging from a fully continuous hybrid monolayer to well-separated Janus nanodots can be obtained. The growth starts with heterogeneous nucleation on morphological defects such as Pt step edges and proceeds by the addition of small clusters formed by the decomposition of the dimethylamino borane complex. Scanning tunneling microscopy measurements indicate that a sharp zigzag in-plane boundary is formed when graphene grows aligned with the Pt substrate and consequently with the h-BN layer as well. When graphene grows rotated by 30°, the graphene armchair edges are seamlessly connected to h-BN zigzag edges. This is confirmed by a thorough density functional theory (DFT) study. Angle Resolved Photoemission Spectroscopy data suggests that both h-BN and graphene present the typical electronic structure of self-standing non-interacting materials

## KEYWORDS

Graphene, h-BN, heterostructures, scanning tunneling microscopy, Density functional theory

Address correspondence to First A. Firstauthor, email1; Third C. Thirdauthor, email2

Nano Research

ISSN 1998-0124 CN 11-5974/O4

https://doi.org/(automatically inserted by the publisher)



## Introduction

The rational combination of different 2D nanosheets to assemble complex hybrid nanocomposites represents a powerful strategy to produce materials with radically innovative and improved properties [1]. This method has made possible the preparation of artificial solids with unique features that can be easily manipulated according to the nature of the materials that are used, and the way they are combined [2,3]. So far two main routes were investigated: the stacking of nanosheets on top of each other by taking advantage of their 2D nature and scarce intralayer Van der Waals interactions [4], or the formation of in-plane heterostructures [5]. The first approach is already well-established as demonstrated by many seminal works [6,7,8] the second is still largely unexplored because of the great challenges associated with the synthesis of interfaces where the atoms of one material are covalently bonded to those of another one, while maintaining a precise structural order [9]. The characterization of such systems is very challenging and requires the use of sophisticated techniques that are able to investigate chemical and structural properties at the atomic level. Nonetheless, 2D heterostructures are currently sparking a great deal of interest: theoretical calculations predict that in-plane interfaces should possess novel electronic [10,11,12,13,14,15] and physicochemical properties [16,17,18,19] which can be the stepping stone for developing new devices and atomically thin circuitry [20,21,22,23]. Therefore, it is of great importance to develop strategies for preparing interfaces engineered at the atomic scale and to characterize their unique properties. Currently, many substrates and several procedures have been used to create lateral heterostructures [9] mostly exploiting heterogeneous nucleation [24] and 2D heteroepitaxy [25] or complex sequential lithography [20] or molecular beam epitaxy based methods [26] On the contrary, truly parallel bottom-up strategies are still extremely rare in the field [10].

Here we demonstrate how to grow a variety of nanohybrids made by forming a lateral heterojunction between graphene and h-BN using a unique precursor bearing carbon nitrogen and boron, i.e. the dimethylamino borane complex (DMAB). By using Scanning Tunneling Microscopy (STM), we were able to identify the growth conditions for the preparation of either full coverage, continuous films, or well-separated h-BN/graphene Janus nanostructures characterized by atomically sharp interfaces involving zigzag/zigzag and newly reported armchair/zigzag graphene/h-BN grain boundaries. These new interfaces have been thoroughly investigated by X-ray Photoemission Spectroscopy (XPS) Angle Resolved Photoemission Spectroscopy (ARPES) and state-of-the-art density functional theory (DFT) calculations.

## Results and discussion

DMAB was used as single precursor for the preparation of h-BN and graphene layers on the Pt(111) surface. Different pressures and temperatures were explored, refining our previous synthesis procedure [27]. As a first step towards gaining an understanding of the growth of a hybrid layer, we have studied the decomposition of the precursor on a single crystal Pt surface as a function of temperature. Thermal Programmed Desorption (TPD) data indicate that on the Pt(111) surface, the DMAB undergoes a first massive dehydrogenation reaction at 270 K (Fig.1). Previous works suggested that in this temperature range in the presence of a catalytic metal, amino-borane adducts undergo de-hydrocoupling and form dimeric cyclic borazanes [28,29]. Also a subsequent $H_2$ desorption that has peaks at 450 K and 588 K is connected to further dehydrogenation processes involving DMAB, since $H_2$ desorbs from Pt(111) between 200 K and 400 K [30]. These additional de-hydrocoupling steps require both the partial elimination of methyl groups, which remain adsorbed on the surface [31] and the formation of variably substituted hexagonal cycloborazanes units that can be considered h-BN precursors [29]. These data indicate that the DMAB in the early stages of its decomposition provide the basis for chemical segregation at the atomic level of h-BN units separated by carbon moieties. At about 580 K, a more extended molecular cracking is observed, resulting in the formation of molecular hydrogen and CN species (m/z=26). This is compatible with the reaction between methyl and ammonia surface species on the Pt(111) with the elimination of hydrogen [32], which is also experimentally detected. Starting from 800 K, the signals from methane(m/z=16), ammonia (m/z=17) and hydrogen are detected, indicating that at this temperature the DMAB molecule and its intermediate decomposition products can be fully dissociated into smaller units containing either only C or N or B. The TPD data suggest that in the deposition condition (> 800 K) on the surface, the most likely species are C, N and B single units or clusters comprising borazanes rings.

The growth of hybrid layers has been investigated by STM at different temperatures and exposure times. At about 800 K, after 2 minutes DMAB exposure at $2\times10^{-8}$ mbar (see Fig. 2), the surface is covered by disordered clusters and large graphene islands (Fig. 2a), and it is possible to resolve the typical Moiré pattern of

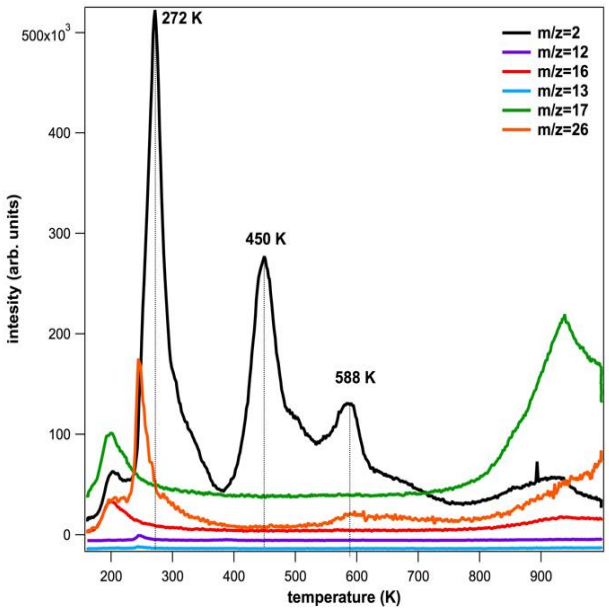


**Fig. 1.** Temperature programmed reaction data of 10 L of DMAB adsorbed at 160 K on the Pt(111) surface and annealed in UHV at 2K/sec to 1000K. The signals corresponding to hydrogen (m/z=2), carbon (m/z=12), methane (m/z=16), Borane (m/z=13), ammonia (m/z=17) and CN (m/z=26) fragments have been recorded with a quadrupole mass spectrum.

graphene on Pt(111) (see Fig. 2b, where the (3×3)R19° superstructure is visible) [33]. The islands start nucleating on the upper rim of the Pt(111) step edges[34] and grow toward the inner part of the terraces, adopting a disordered wave front that does not follow a specific crystallographic direction and terminates with randomly arranged bright spots, as expected for attachment-limited growth [35,36].

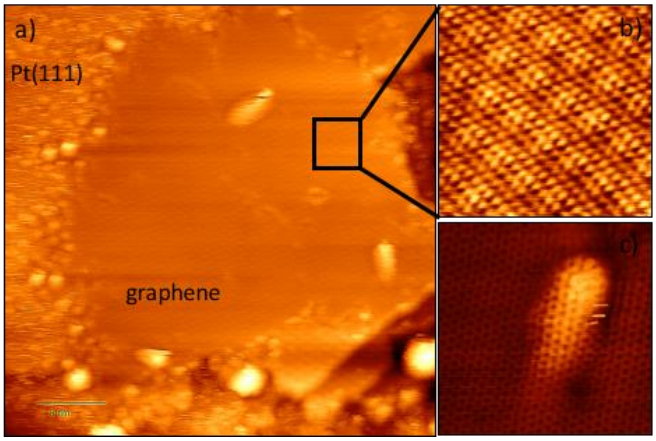


**Fig 2**. STM images of the Pt(111) surface after dosing DMAB at 800 K for 2'at $2\times10^{-8}$ mbar a) large scale morphology, b) atomic resolution of the (4×4)R14° Moiré pattern inside the graphene islands, c) magnified view of one of the dome-like features that can be observed in the middle of graphene patches.

The graphene islands often exhibit peculiar morphological features that consist of dome-like structures characterized by a corrugation of about 3-4 Å high, (Fig. 2c). On these large protrusions, it is possible to resolve a hexagonal pattern that, on the very top, is highly distorted, but on the sides, matches perfectly with that of the surrounding graphene layer. Recently, similar morphological features structures have been observed during the early stages of the graphene growth on Pt(111) at 850 K, using ethylene as carbon source [37]. When compared with DFT model calculations, these structures were found to be associated with graphene islands where only the edges interact with the substrate, while the remaining atoms are suspended forming bowl-like structures [37]. At variance with the morphological disorder observed close to the edges, the internal parts of graphene islands are very ordered. Atomically resolved images indicate the presence of very few defects, which according to data in the literature can be associated mostly with single atom N dopants, (see figure S1) [38,39].

If the growth is continued for longer times (up to 30 minutes), the surface becomes fully covered by graphene patches 30-50 nm wide that are separated by highly disordered regions formed by the aggregation of 3D clusters. At this stage, the observed LEED pattern (not shown) is a mixture of different graphene superstructures that result in a diffused ring. Notably, there is no trace of the h-BN (9×9) superstructure [40].

XPS measurements (see Supporting Information Fig. S2) show the presence of several chemically shifted components in the C 1*s*, B 1*s* and N 1*s* core levels spectra, indicating the formation of disordered carbon-boron-nitride alloys. However, the analysis of the C 1*s* photoemission line indicates that the most intense component, which accounts for 63% of the total intensity, is associated with C $sp^2$ [31]. From XPS data, we deduce an elemental composition of $B_{0.26}C_{0.41}N_{0.33}$. The information provided by photoemission measurements, combined with the observed morphology and TPD data, suggest that when DMAB is dosed at 800 K, a graphene layer can be formed by the nucleation of small carbon clusters, whereas the B and N atoms or cyclic borazane units are not effectively attached to the growing graphene patch and remain on the surfaces forming disordered 3D clusters. As a matter of fact, the attachment of carbon atoms to the growing edge is one of the possible rate determining steps controlling the growth of graphene [41,36]. Interestingly, the graphene edges are able to sort out the type of atoms that can be added to the growing islands. This atom selection is in line with theoretical calculations that indicate both on the basis of thermodynamic data [42] and considerations of bond conjugation and aromaticity [43] that graphene and h-BN should preferentially form separated phases.

When the growth temperature approaches 1000 K, it is possible to observe also the nucleation of h-BN islands as confirmed by microscopy and diffraction data. The corresponding LEED pattern (Fig. S3) shows the presence of the (9×9) reconstruction of h-BN and the formation of a diffused intensity ring due to azimuthally

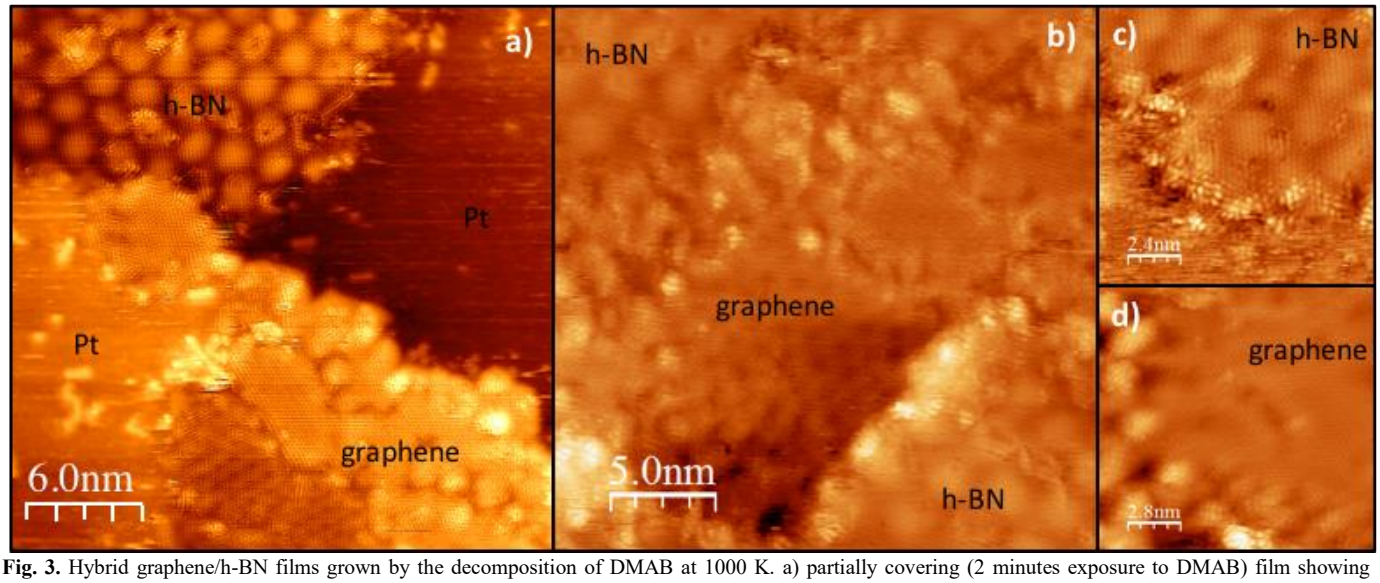


**Fig. 3.** Hybrid graphene/h-BN films grown by the decomposition of DMAB at 1000 K. a) partially covering (2 minutes exposure to DMAB) film showing preferential nucleation at the step edges b) fully continuous film presenting h-BN and graphene patches with disordered areas where the two materials merge c) details of h-BN and d) graphene island edges.

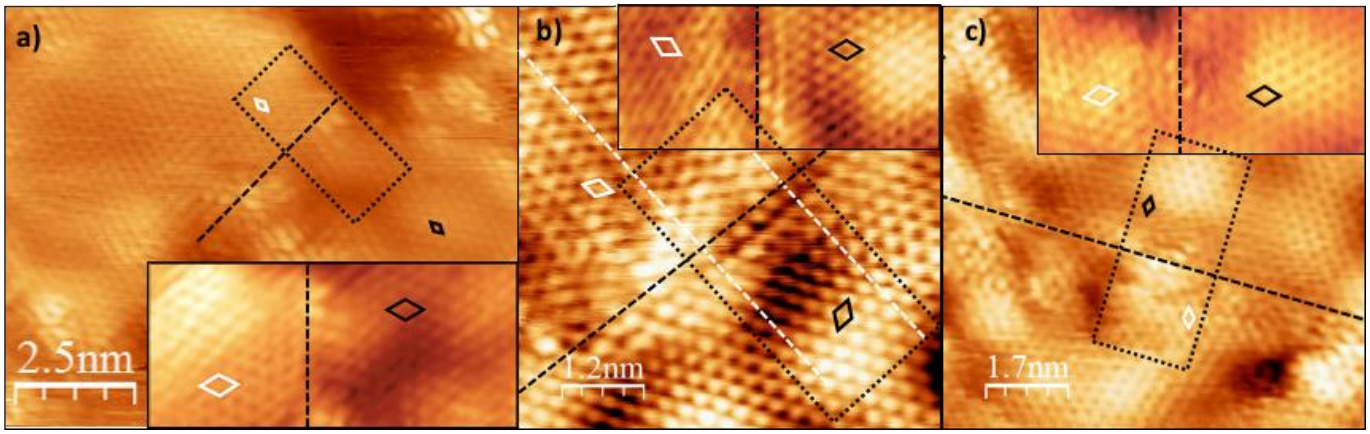


**Fig. 4.** In-plane boundaries (dashed black lines) between h-BN and graphene: a) the angle between the graphene and h-BN lattice is 0° a), 30° b) and 14°c). The white (black) rhombus corresponds to the graphene (h-BN) unit cell. The insets are enlarged views of the area included in the dotted rectangles.

rotated graphene domains. An enhancement of the diffracted intensity can be observed at 0° and 30° with respect to the <110> Pt directions, indicating that some graphene domains are preferentially formed [33].

The XPS measurements corroborate the diffraction and microscopy data. The C 1*s* photoemission spectrum shows a distinctive sharp peak at 284.1 eV assigned to $sp^2$ hybridized C atoms in graphene [44], which accounts for 81% of the whole intensity (Fig. S4). Some components due to C-B and C-N bonds are visible, but are relatively less intense than in the lower temperature preparation, (Fig. S2). B 1*s* and N 1*s* core levels are also much narrower and with a spectral fingerprint compatible with *h*-BN/Pt(111) layers. The weak components at higher BE are assigned to a minority $sp^3$ $BN_x$ species [40], and to the presence of the aforementioned bonds with carbon in the case of N 1s, or to $BO_x$ bond in the case of B 1s [31]. The elemental composition of the layer resulted $C_{0.59}$ $B_{0.18}N_{0.19}O_{0.04}$, where the oxygen is due to the atmosphere exposure after the growth.

The STM images taken at the early stages of growth at 1000 K (2 minutes at $10^{-8}$ mbar) show the formation of distinct patches of graphene and h-BN, which can be easily distinguished based on the peculiar modulation of their moiré pattern and different orientation of their atomic lattices. Heterogeneous nucleation is strongly favoured, but with differences between graphene and h-BN: the former prefers to nucleate on the upper rim of Pt steps whereas the latter on the lower one, (Fig. 3a). Atomically resolved STM images indicate that the edges of both h-BN and graphene islands are very defective, being characterized by bright bumps that often deviate from a hexagonal arrangement (see Fig. 3c,d). Therefore it seems that the growth mechanism entails the progressive addition of atoms or small clusters provided by the larger particles that can be observed on the uncovered Pt(111) surface. When the exposure time is increased to 30 minutes, a continuous patched layer of graphene and h-BN is eventually formed (Fig. 3b), even if at the boundaries between the two materials some rough disordered areas can be observed. CO titration measurements indicate that despite the local defectivity and complexity of the junctions between the h-BN and graphene, no Pt atoms are exposed [27].

From the crystallographic point of view, different interfaces can be observed. As suggested by the macroscopic LEED pattern (Fig. S3), the h-BN is always oriented with the Pt(111) substrate, whereas graphene can adopt several orientations, but the most likely ones are those aligned with Pt or rotated by 30°. Atomically resolved STM images of these heterostructures are presented in Fig. 4. When both materials are aligned with the Pt substrate, the interface runs along the zigzag direction (see Fig. 4a); this 2D epitaxial matching is that most commonly observed in the literature, and was found on other h-BN/graphene lateral heterostructures supported on Ir(111) [45], Cu(111) [46], Rh(111) [47]. In contrast, when graphene is rotated by 30° a commensurate interface can be observed, which entails the coupling of armchair graphene with zigzag h-BN edges. In this case, six graphene units (6×2.13=12.78 Å) are matched with 5 of h-BN (5×2.52=12.6 Å), resulting in a minimum strain (1.4%) even lower than the simple zigzag/zigzag matching, although it requires the formation of 5 and 7 member rings as also reported in the case of the grain boundaries of h-BN on Cu(111), (*vide infra*) [48]. The interface is quite sharp, but strong variations of the STM contrast atomic and notable deviations from the positions expected for a perfect

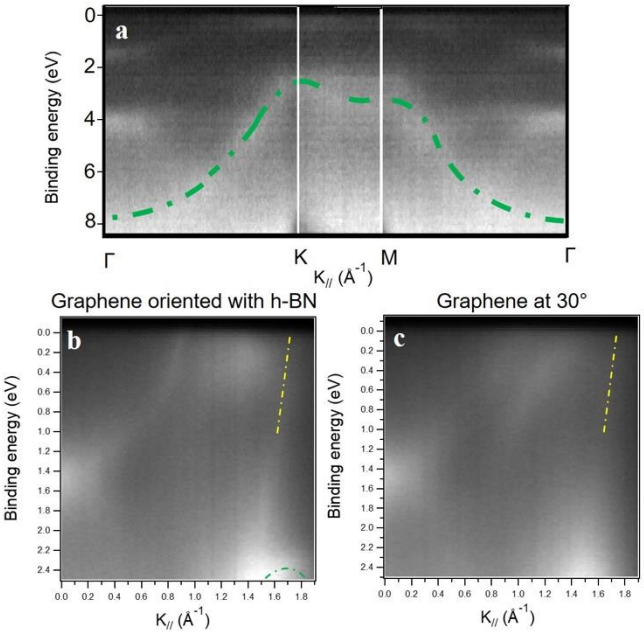


**Fig. 5** ARPES acquisition of graphene h-BN heterostructure synthesized at 1000 K. a) wide energy acquisition to distinguish the h-BN electronic structure in the high symmetry directions. The green dashed line is a guide for the eyes. b-c) Wave-vector vs energy high-resolution profiles close to the Fermi edge. b) Γ to K cut parallel to h-BN K point, c) cut at 30° to h-BN K point (i.e. h-BN M point). The green and yellow dashed lines are a guide for the eyes for the position of h-BN band at the K point and graphene π band, respectively.

hexagonal structure can be observed on the graphene side. This is a general trait of all interfaces: the h-BN side is minimally affected,

while the graphene side, is both electronically and geometrically perturbed. Since graphene can adopt several orientations, also low angle boundaries characterized by the absence of ordered structures can be formed, as reported in Fig. 4c, which shows the formation of an interface between h-BN and a graphene domain rotated by 14°. Also here it may be seen that the h-BN side is slightly perturbed with only minor changes in the moiré periodicity, whereas the graphene side is very defective.

Quite interestingly, when the surface is flash exposed to DMAB (about 5 seconds) and then annealed in UHV at 1000 K for 25 minutes, the morphology is radically different: instead of large patches, small well-separated islands are formed, which are less than 10 nm wide (Fig. S4). Notably, most of these "quantum dots" are made by two moieties: h-BN and graphene such as in Fig. 4a, representing special Janus heterostructures.

The electronic properties of the graphene/h-BN heterostructures obtained at 1000 K were investigated by ARPES. The measurements were quite challenging because of the small dimensions of the graphene domains; however, it was possible to distinguish the spectroscopic features in the whole k-space of both graphene and h-BN by means of all wave-vector parallel ARPES acquisitions acquired by Photo Electron Emission Microscopy (PEEM). In Fig. 5a we report the energy vs momentum dispersion of h-BN along high symmetry directions. The positions of the bands are the same as those observed for pure h-BN/Pt(111) [49,50] which is distinctive of a non-interacting system.

On the other hand, the signal coming from graphene is less intense than that of h-BN, even if the graphene covers about 60% of the surface. This is due to the presence of differently oriented domains as documented by STM and LEED. Interestingly, the linear portion of the π band close to the K point is more visible when the graphene is oriented with h-BN (Fig. 5b), while showing lower intensity when rotated at 30° (Fig. 5c). This is the first time that the band dispersion in the valence band of graphene patches orientated with the main directions of the Pt(111) crystal has been measured, instead of the ARPES more usually reported, which pertains to the superstructure rotated by 30° [44,51,52,53] The full wave-vector ARPES data clearly prove the presence of graphene oriented with h-BN on a large scale, which occurs due to a 2D heteroepitaxial growth favoured by the h-BN edges [25,54].

Because of its weak intensity, it is not possible to clearly visualize the Dirac cones. However, by the extrapolation of the intensity of the π band, we can estimate a doping level close to zero for graphene oriented with *h*-BN as well as rotated by 30°. Recently a hole doping of 0.44 eV has been found for graphene growth at similar temperatures to this work on the Pt(111) surface [51]. The negligible doping observed in the present case is related to the presence of h-BN in the heterostructures, also the slight excess of N in the overall composition of the film, which may point to an excess presence of n-dopants that may counterbalance the electron transfer to the substrate [55].

Since this is the first time that a zigzag h-BN/armchair graphene interface has been identified (in the following simply zz-BN/a-G ), and considering its importance as a possible new element for the development of atomically thin circuitry, we investigated using density functional theory calculations, its structure and electronic properties. We considered several approaches in order to model this special lateral interface: as a neutral and as a negatively charged system These are presented in Figures S6 and S7. The h-BN edge of a nanoribbon can face the edge of a graphene nanoribbon with a B or an N row of atoms. We proved that, in all the investigated cases, the B/C interface (a, b, c in Figure S6) is more stable than the N/C one (d, e, f in Figure S6). The most stable neutral configuration, which will be considered in this work, is shown in Figure 6a. This is characterized by a C vacancy at the interface that allows saturation of all the B-C bonds in the basal plane. However, one π state is not full, but only half-filled (see the position of the Fermi level in the density of states (DOS) and the band state crossing the Fermi energy in the band structure of Figure S8, as obtained with both vdW-DF2$^{C09x}$/QE and B3LYP/CRY14 calculations), leaving a delocalized hole in the system (shown as a yellow charge density plot in Figure 6a). Adding an extra electron to this model simply fills the hole state (Figure S7a). As a next step, we deposited the neutral model of the zz-BN/a-G interface on the Pt (111) surface and performed atomic relaxation. The optimized structure is shown in Figure 6b. We observe a double arching of the nanoribbon with some enhanced interaction at the interfacing atoms (B and C) and at the borders, especially in the case of the graphene side. Since we believe that this effect is partly due to the hole present in the ribbon, we added an extra electron to the system to heal the hole. However, we observe that this extra electron does not fill the hole, but goes into the metal. Therefore, even a negatively charged calculation is still characterized by the same arching of the nanoribbon. We attribute this curvature in the hybrid structure (i) to the C/Pt hybridization as a consequence of the hole state and (ii) to the limited width of the ribbon, since we observe that the thinner the nanoribbon, the larger the effect. We also analyzed the charge transfer between the zz-BN/a-G interface and the metal support (see Figure S9). We observe some electron charge depletion on those metal atoms that are more in contact with the nanoribbon and some electron charge accumulation in the space between the metal and the C atoms of the nanoribbon closer to the surface. The electronic structure of the nanoribbon is quite modified by the presence of the metal surface, as we can observe by comparing Figure S8a and Figure S10a, with some N $p_z$ states from the h-BN (blue line) shifting towards the Fermi energy.

There is little contribution by the B atoms to the mixing with the metal state, as one can conclude from both the DOS (Figure S10a) and the projected band structures (Figure S10b). Then, we performed STM image simulation and compared the result with the experimental one in Figure 7. Note that various bias voltage values have been considered, as documented in Figure S11. The simulated STM image of the model proposed very nicely resembles the experimental one.

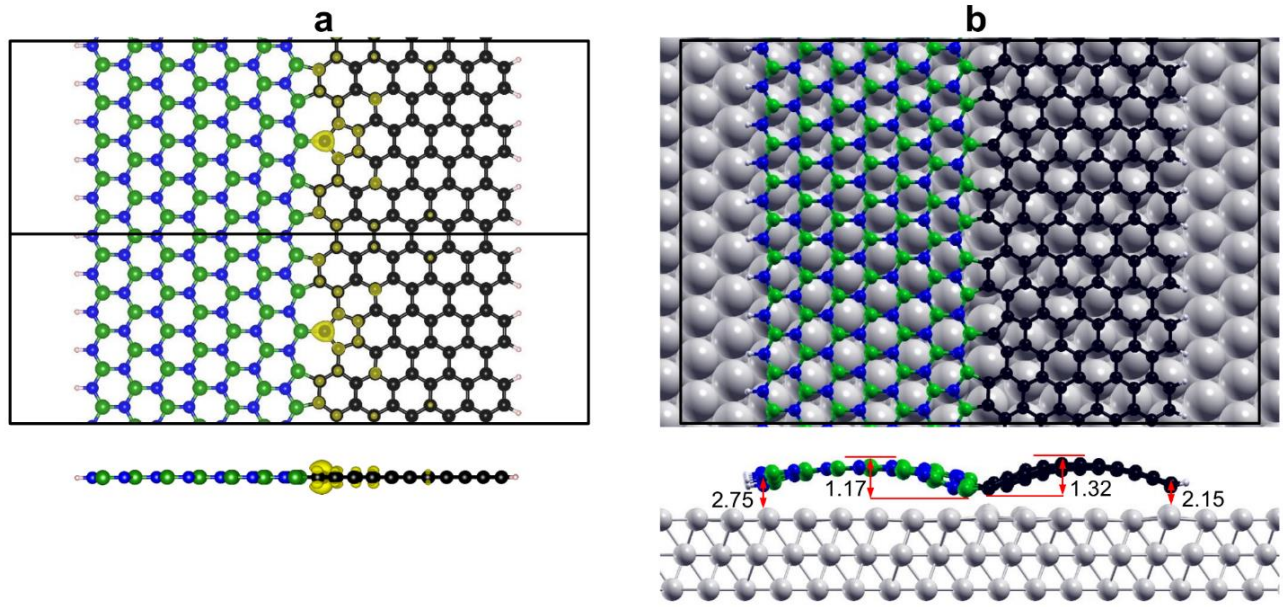


**Figure 6**: (a) Top and side views for the free standing zz-BN/a-G interface with the charge density plot of the half-filled band shown in Figure S4. The cell has been repeated twice along the periodic direction. The iso-surface value is set to 0.01 $e^{-}/Å^{3}$. (b) Top and side views for the Pt (111) supported zz-BN/a-G interface. The corrugation of the interface is labelled in the side view (in Å). Color coding: B atoms in green; N atoms in blue; C atoms in black; H atoms in white and Pt atoms in grey.

Nano Research
ISSN 1998-0124 CN 11-5974/O4
https://doi.org/(automatically inserted by the publisher)



Finally, we tried to compare the stability of the zz-BN/a-G interface with the more common zigzag h-BN/zigzag graphene one (later on zz-BN/zz-G, shown in Figure S12). This comparative analysis is not straightforward since the number of atom is not exactly the same. Therefore, we present an energy of formation that has been normalized with the length of the nanoribbon, as defined in the computational methods: it is +0.71 eV/Å with respect to +0.52 eV/Å, for the zz-BN/a-G and the zz-BN/zz-G interfaces, respectively.

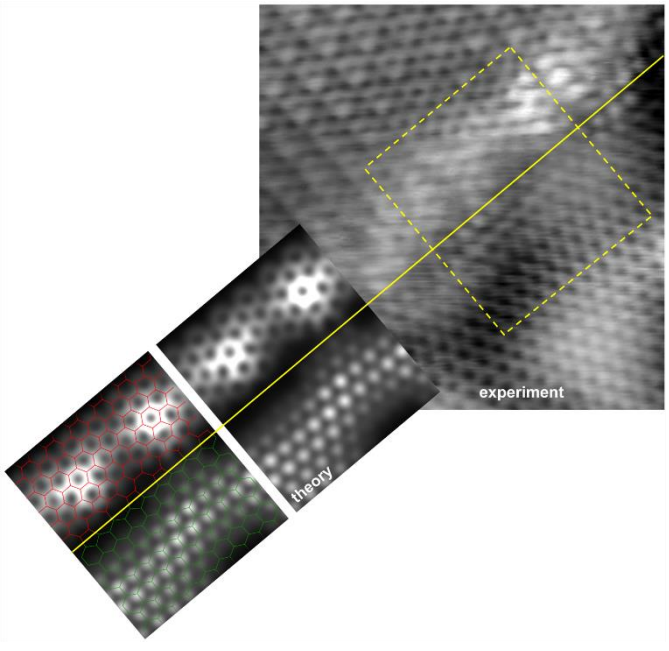


**Figure 7**: Experimental (on the right) and simulated (in the middle and on the left) STM images for the Pt (111) supported zz-BN/a-G interface. On the left, the stick model for zz-BN/a-G interface is superimposed on the simulated STM image. Color coding: h-BN in green, graphene in red. The bias voltage is -1.5 V.

## Conclusions

We have shown that by using a single source precursor a variety of hybrid layers composed of graphene and h-BN can be prepared. Since on the Pt(111) surface, graphene can grow according to different rotational angles, whereas h-BN is pinned to a unique direction (i.e. aligned with the substrate), several different combinations of in-plane lateral heterostructures can be formed. In particular, we reported for the first time the existence of a linear boundary where the armchair edge of graphene connects with the zigzag edge of h-BN. This special interface has been thoroughly investigated by first-principles calculations, elucidating their structure and electronic properties. A nice agreement between simulated and experimental STM images has been observed. The presence of unusually abundant graphene domains oriented with Pt(111) surface has been proven by ARPES macroscopic acquisition. We also show that by varying the deposition conditions very small h-BN/graphene Janus nanodots can be formed with a high yield. Furthermore, the large density of interfaces that can be obtained by this synthesis protocol, provides the ideal material platform for studying the catalytic properties of in-plane heterostructures[16,17,18,56,57], and their defectivity[58].

## Materials and Methods

### Experimental

Dimethylamine borane (DMAB, 97% Sigma-Aldrich) was used as the source for carbon, boron and nitrogen for the growth of 2D nanohybrids. Prior to the experiment, the precursor was degassed for several hours at 41 °C. A clean and ordered Pt(111) surface was obtained after cycles of $Ar^+$ sputtering and annealing at 700 °C. DMAB vapors were dosed onto Pt(111) in the range of temperature from 800 to 1000 K. After cooling down to room temperature (RT), the sample was examined by a VT Omicron STM. The TPR measurements were acquired with a HIDEN quadrupole mass spectrometer, covered by gas-tight quartz shield terminating with a 6 mm hole in proximity of the ionization gauge, which was brought close (2 mm) to the sample surface. The sample was fixed through two tantalum wires to a manipulator that could be cooled down to 120 K. The desorption spectra were acquired with a heating rate of 2K/sec. The ARPES spectra were acquired with a NanoESCA II Energy -filtered PEEM using a non-monochromatic He I (21.2 eV) source at room temperature from a field of view of approximatively 80 µm with a 107 meV overall energy resolution. The XPS spectra were collected in a UHV systems equipped with a VG Escalab MK II electron spectrometer using a non monochromated mg x-ray source.

### Computational methods

The lateral *h*-BN/graphene interface is constructed by merging a half *h*-BN domain and a half graphene domain into one supercell. Different interfaces occur depending on the misorientation angle between *h*-BN lattice and graphene lattice. Here two kinds of interfaces were modeled, including zigzag *h*-BN/zigzag graphene (zz-BN/zz-G) and zigzag *h*-BN/armchair graphene (zz-BN/a-G). For each kind of interface, the interface can be either B-C bonded or N-C bonded. For the zz-BN/zz-G interface, a zigzag *h*-BN nanoribbon unit cell with 7 zigzag chains across the ribbon width and a zigzag graphene nanoribbon unit cell with 7 zigzag chains are merged (shown in Figure S12 in the ESI). The zz-BN/a-G interface was constructed by merging five units of zigzag *h*-BN nanoribbon with 7 zigzag chains and three units of armchair graphene nanoribbon with 11 C-C dimer lines across the ribbon width (shown in Figure S6). The mismatch is 2.0%. The edges of all the h-BN/graphene interfaces are saturated by hydrogen atoms. Both atomic positions and lattice parameters for all the interfaces were fully relaxed.

The thermodynamic stability of an interface can be characterized by its formation energy ($E_{form}$) defined as the energy penalty per unit length along the interface[59,14,60]:

$$E_{form} = (E_{tot} - N_C E_C - N_{BN} E_{BN} - N_H E_H)/L,$$

where $E_{tot}$ is the total energy of the interface. $E_C$, $E_{BN}$ and $E_H$ are the energy per carbon for the pristine graphene, energy per BN atom pair for the pristine *h*-BN monolayer and energy per H for isolated $H_2$ molecule. $N_C$, $N_{BN}$ and $N_H$ are the number of carbon atoms, BN atom pairs and H atoms in the interface supercell, respectively. L is the periodic length along the interface.

The Pt(111) surface was modeled by a three-layer slab model with the bottom layer fixed during the geometry relaxation to mimic a semi-infinite solid. To avoid interactions between adjacent periodic images, a vacuum space of more than 11 Å was included in the slab model. The Pt(111) supported zz-BN/a-G interface was modeled by putting a free-standing zz-BN/a-G interface supercell with 2 unit cells in the periodic direction on a (8 × 9) supercell of the rectangular Pt(111) unit cell. The lattice parameter for the free-standing zz-BN/a-G interface supercell (25.31 Å) was adopted stretching the Pt(111) surface by 1.2%.

DFT calculations were mainly performed using the plane-wave-

based Quantum ESPRESSO package [60]. The ultrasoft pseudopotentials were adopted to describe the electron-ion interactions with Pt (5d, 6s), B (2s, 2p), N (2s, 2p), C (2s, 2p), H (1s), treated as valence electrons. To properly take into account weak interactions, the van der Waals density functional vdW-DF2$^{C09x}$ [61], which has been reported to have good overall performances for adsorption distances of graphene on metal surfaces, was used. Energy cutoffs of 30 Ryd and 240 Ryd (for kinetic energy and charge density expansion, respectively) were adopted for all calculations. The convergence criterion of 0.026 eV/Å for force was used during geometry optimization and the convergence criterion for total energy was set at $10^{-6}$ Ryd. The STM images for the Pt(111) supported zz-BN/a-G interface were simulated by using the Tersoff-Hamann approximation[62] with a constant height of 2.5 Å above the top atom.

Hybrid functional calculations (B3LYP[63,64]) were carried out for the free-standing zz-BN/a-G interface using the CRYSTAL14 package [65,66] to compare the results with those from PBE. The all-electron basis sets are H|5-11(p1), B|6-24++(d1), N|6-24++(d1) and C|6-31(d1). The convergence criterion of 0.023 eV/Å for force was used during geometry optimization and the convergence criterion for total energy was set at $10^{-6}$ Hartree.

The geometry relaxation of free-standing zz-BN/a-G and zz-BN/zz-G interfaces was performed with Monkhorst−Pack k-points mesh of 1 × 8 × 1 and 1 × 72 × 1, respectively. For electron density of states of zz-BN/a-G interface, k-points mesh of 1 × 22 × 1 was used. A k-points mesh of 2 × 3 × 1 was used for Pt(111) supported zz-BN/a-G interface.

## Acknowledgements

This work was partially supported by the Italian MIUR through the national grant Futuro in Ricerca 2012 RBFR128BEC “Beyond graphene: tailored C-layers for novel catalytic materials and green chemistry”. Authors acknowledge access to the Bristol NanoESCA Facility (EPSRC Strategic Equipment Grant EP/K035746/1 and EP/M000605/1).

## Electronic Supplementary Material

Supplementary materials: additional STM images, LEED pattern of the h-BN graphene films grown at 1000 K, multipeak analysis of the C 1s, B 1s, N 1s photoemission spectra, additional DFT calculations (pDOS, STM images simulations).

## References

[1] Bonaccorso, F.; Colombo, L.; Yu, G.; Stoller, M.; Tozzini, V.; Ferrari, a C.; Ruoff, R. S.; Pellegrini, V. 2D Materials. Graphene, Related Two-Dimensional Crystals, and Hybrid Systems for Energy Conversion and Storage. *Science* **2015**, *347*, 1246501.

[2] Jariwala, D.; Marks, T. J.; Hersam, M. C. Mixed-Dimensional van Der Waals Heterostructures. *Nat. Mater.* **2016**, *16*, 170–181.

[3] Das, S.; Robinson, J. A.; Dubey, M.; Terrones, H.; Terrones, M. Beyond Graphene: Progress in Novel Two-Dimensional Materials and van Der Waals Solids. *Annu. Rev. Mater. Res.* **2015**, *45*, 1–27.

[4] Novoselov, K. S.; Mishchenko, A.; Carvalho, A.; Castro Neto, A. H. 2D Materials and van Der Waals Heterostructures. *Science* **2016**, *353*, aac9439.

[5] Duong, D. L.; Yun, S. J.; Lee, Y. H. Van Der Waals Layered Materials: Opportunities and Challenges. *ACS Nano* **2017,** *11*, 1180.

[6] Lee, J.; Shin, J.-H.; Lee, G.-H.; Lee, C.-H. Two-Dimensional Semiconductor Optoelectronics Based on van Der Waals Heterostructures. *Nanomaterials* **2016**, *6*, 193.

[7] Geim, A. K.; Grigorieva, I. V. Van Der Waals Heterostructures. *Nature* **2013**, *499*, 419–425.

[8] Cattelan, M.; Markman, B.; Lucchini, G.; Das, P. K.; Vobornik, I.; Robinson, J. A.; Agnoli, S.; Granozzi, G. New Strategy for the Growth of Complex Heterostructures Based on Different 2D Materials. *Chem. Mater.* **2015**, *27*, 4105.

[9] Solís-Fernández, P.; Bissett, M.; Ago, H. Synthesis, Structure and Applications of Graphene-Based 2D Heterostructures. *Chem. Soc. Rev.* **2017**, *46*, 4572–4613.

[10] Gong, Y.; Lin, J.; Wang, X.; Shi, G.; Lei, S.; Lin, Z.; Zou, X.; Ye, G.; Vajtai, R.; Yakobson, B. I.; Terrones, H.; Terrones, M.; Tay, B. K.; Lou, J.; Pantelides, S. T.; Liu, Z.; Zhou, W.; Ajayan, P. M. Vertical and in-Plane Heterostructures from $WS_2$/$MoS_2$ Monolayers. *Nat. Mater.* **2014**, *13*, 1135.

[11] Zhang, J.; Xie, W.; Zhao, J.; Zhang, S. Band Alignment of Two-Dimensional Lateral Heterostructures. *2D Mater.* **2017**, *4*, 15038.

[12] Drost, R.; Uppstu, A.; Schulz, F.; Hämäläinen, S. K.; Ervasti, M.; Harju, A.; Liljeroth, P. Electronic States at the Graphene - Hexagonal Boron Nitride Zigzag Interface. *Nano Lett.* **2014**, *14*, 5128–5132.

[13] Sun, Q.; Dai, Y.; Ma, Y.; Wei, W.; Huang, B. Lateral Heterojunctions within Monolayer H-BN/graphene: A First-Principles Study. *RSC Adv.* **2015**, *5* (42), 33037–33043.

[14] Zhang, J.; Xie, W.; Xu, X.; Zhang, S.; Zhao, J. Structural and Electronic Properties of Interfaces in Graphene and Hexagonal Boron Nitride Lateral Heterostructures. *Chem. Mater.* **2016**, *28*, 5022–5028.

[15] Yu, Z. G.; Zhang, Y. W. Electronic Properties of Mutually Embedded H-BN and Graphene: A First Principles Study. *Chem. Phys. Lett.* **2016**, *666*, 33–37.

[16] Krsmanović, R. S.; Šljivančanin, Ž. Atomic Structure, Electronic Properties, and Reactivity of in-Plane Heterostructures of Graphene and Hexagonal Boron Nitride. *J. Phys. Chem. C* **2014**, *118*, 16104–16112.

[17] Nguyen, M.-T. Reactivity of Graphene and Hexagonal Boron Nitride In-Plane Heterostructures with Oxygen: A DFT Study. *ChemPhysChem* **2014**, *15*, 2372–2376.

[18] Li, M.; Wang, Y.; Tang, P.; Xie, N.; Zhao, Y.; Liu, X.; Hu, G.; Xie, J.; Zhao, Y.; Tang, J.; Zhang, T.; Ma, D. Graphene with Atomic-Level In-Plane Decoration of H-BN Domains for Efficient Photocatalysis. *Chem. Mater.* **2017**, *29*, 2769–2776.

[19] Chen, X. K.; Hu, J. W.; Wu, X. J.; Jia, P.; Peng, Z. H.; Chen, K. Q. Tunable Thermal Rectification in Graphene/hexagonal Boron Nitride Hybrid Structures. *J. Phys. D. Appl. Phys.* **2018**, *51,* 085103.

[20] Liu, Z.; Ma, L.; Shi, G.; Zhou, W.; Gong, Y.; Lei, S.; Yang, X.; Zhang, J.; Yu, J.; Hackenberg, K. P.; Babakhani, A.; Idrobo, J. C.; Vajtai, R.; Lou, J.; Ajayan, P. M. In-Plane Heterostructures of Graphene and Hexagonal Boron Nitride with Controlled Domain Sizes. *Nat. Nanotechnol.* **2013**, *8*, 119–124.

[21] Levendorf, M. P.; Kim, C. J.; Brown, L.; Huang, P. Y.; Havener, R. W.; Muller, D. A.; Park, J. Graphene and Boron Nitride Lateral Heterostructures for Atomically Thin Circuitry. *Nature* **2012**, *488*, 627–632.

[22] Huang, C.; Wu, S.; Sanchez, A. M.; Peters, J. J. P.; Beanland, R.; Ross, J. S.; Rivera, P.; Yao, W.; Cobden, D. H.; Xu, X. Lateral Heterojunctions within Monolayer $MoSe_2$-$WSe_2$ Semiconductors. *Nat. Mater.* **2014**, *13*, 1096–1101.

[23] Zhang, S.; Li, J.; Wu, H.; Li, X.; Guo, W. Direct Synthesizing In-Plane Heterostructures of Graphene and Hexagonal Boron Nitride in Designed Pattern. *Adv. Mater. Interfaces* **2018**, *5*, 1800208.

[24] Zhang, X. Q.; Lin, C. H.; Tseng, Y. W.; Huang, K. H.; Lee, Y. H. Synthesis of Lateral Heterostructures of Semiconducting Atomic

Layers. *Nano Lett.* **2015**, *15*, 410–415.

[25] Liu, L.; Park, J.; Siegel, D. A.; McCarty, K. F.; Clark, K. W.; Deng, W.; Basile, L.; Idrobo, J. C.; Li, A. P.; Gu, G. Heteroepitaxial Growth of Two-Dimensional Hexagonal Boron Nitride Templated by Graphene Edges. *Science* **2014**, *343*, 163–167.

[26] Li, M.-Y.; Shi, Y.; Cheng, C.-C.; Lu, L.-S.; Lin, Y.-C.; Tang, H.-L.; Tsai, M.-L.; Chu, C.-W.; Wei, K.-H.; He, J.-H.; Chang, W.-H.; Suenaga, K.; Li, L.-J. Epitaxial Growth of a Monolayer WSe2-MoS2 Lateral P-N Junction with an Atomically Sharp Interface. *Science* **2015**, *349*, 524–528.

[27] Nappini, S.; Píš, I.; Menteş, T. O.; Sala, A.; Cattelan, M.; Agnoli, S.; Bondino, F.; Magnano, E. Formation of a Quasi-Free-Standing Single Layer of Graphene and Hexagonal Boron Nitride on Pt(111) by a Single Molecular Precursor. *Adv. Funct. Mater.* **2016**, *26*, 1120–1126.

[28] Jaska, C. A.; Temple, K.; Lough, A. J.; Manners, I. Transition Metal-Catalyzed Formation of Boron−Nitrogen Bonds: Catalytic Dehydrocoupling of Amine-Borane Adducts to Form Aminoboranes and Borazines. *J. Am. Chem. Soc.* **2003**, *125*, 9424–9434.

[29] Bowden, M. E.; Brown, I. W. M.; Gainsford, G. J.; Wong, H. Structure and Thermal Decomposition of Methylamine Borane. *Inorganica Chim. Acta* **2008**, *361*, 2147–2153.

[30] Christmann, K.; Ertl, G.; Pignet, T. Adsorption of Hydrogen on a Pt(111) Surface. *Surf. Sci.* **1976**, *54*, 365–392.

[31] Nappini, S.; Píš, I.; Carraro, G.; Celasco, E.; Smerieri, M.; Savio, L.; Magnano, E.; Bondino, F. On-Surface Synthesis of Different Boron–nitrogen–carbon Heterostructures from Dimethylamine Borane. *Carbon N. Y.* **2017**, *120*, 185–193.

[32] Herceg, E.; Trenary, M. Formation of Surface CN from the Coupling of C and N Atoms on Pt(111). *J. Am. Chem. Soc.* **2003**, *125* (51), 15758–15759.

[33] Gao, M.; Pan, Y.; Huang, L.; Hu, H.; Zhang, L. Z.; Guo, H. M.; Du, S. X.; Gao, H. J. Epitaxial Growth and Structural Property of Graphene on Pt(111). *Appl. Phys. Lett.* **2011**, *98,* 033101.

[34] Feng, X.; Wu, J.; Bell, A. T.; Salmeron, M. An Atomic Scale View of the Nucleation and Growth of Graphene Islands on Pt Surfaces. *J. Phys. Chem. C* **2015**, *119*, 7124–7129.

[35] Bauer, M.; Bernard, D. 2D Growth Processes: SLE and Loewner Chains. *Physics Reports*. **2006**, *432*, 115–221.

[36] Loginova, E.; Bartelt, N. C.; Feibelman, P. J.; McCarty, K. F. Evidence for Graphene Growth by C Cluster Attachment. *New J. Phys.* **2008**, *10,* 093026.

[37] Kim, H. W.; Ko, W.; Ku, J.; Kim, Y.; Park, S.; Hwang, S. Evolution of Graphene Growth on Pt(111): From Carbon Clusters to Nanoislands. *J. Phys. Chem. C* **2017**, *121*, 25074–25078.

[38] Lambin, P.; Amara, H.; Ducastelle, F.; Henrard, L. Long-Range Interactions between Substitutional Nitrogen Dopants in Graphene: Electronic Properties Calculations. *Phys. Rev. B* **2012**, *86*, 045448.

[39] Zhao, L.; He, R.; Rim, K. T.; Schiros, T.; Kim, K. S.; Zhou, H.; Gutiérrez, C.; Chockalingam, S. P.; Arguello, C. J.; Pálová, L.; Nordlund, D.; Hybertsen, M. S.; Reichman, D. R.; Heinz, T. F.; Kim, P.; Pinczuk, A.; Flynn, G. W.; Pasupathy, A. N. Visualizing Individual Nitrogen Dopants in Monolayer Graphene. *Science* **2011**, *333*, 999–1003.

[40] Ćavar, E.; Westerström, R.; Mikkelsen, A.; Lundgren, E.; Vinogradov, A. S.; Ng, M. L.; Preobrajenski, A. B.; Zakharov, A. A.; Mårtensson, N. A Single H-BN Layer on Pt(1 1 1). *Surf. Sci.* **2008**, *602*, 1722–1726.

[41] Kim, H.; Mattevi, C.; Calvo, M. R.; Oberg, J. C.; Artiglia, L.; Agnoli, S.; Hirjibehedin, C. F.; Chhowalla, M.; Saiz, E. Activation Energy Paths for Graphene Nucleation and Growth on Cu. *ACS Nano* **2012**, *6*, 3614–3623.

[42] Lu, J.; Zhang, K.; Liu, X. F.; Zhang, H.; Sum, T. C.; Neto, A. H. C.; Loh, K. P. Order-Disorder Transition in a Two-Dimensional Boron-Carbon-Nitride Alloy. *Nat. Commun.* **2013**, *4*, 681.

[43] Zhu, J.; Bhandary, S.; Sanyal, B.; Ottosson, H. Interpolation of Atomically Thin Hexagonal Boron Nitride and Graphene: Electronic Structure and Thermodynamic Stability in Terms of All-Carbon Conjugated Paths and Aromatic Hexagons. *J. Phys. Chem. C* **2011**, *115*, 10264–10271.

[44] Cattelan, M.; Peng, G. W.; Cavaliere, E.; Artiglia, L.; Barinov, A.; Roling, L. T.; Favaro, M.; Píš, I.; Nappini, S.; Magnano, E.; Bondino, F.; Gavioli, L.; Agnoli, S.; Mavrikakis, M.; Granozzi, G. The Nature of the Fe-Graphene Interface at the Nanometer Level. *Nanoscale* **2015**, *7*, 2450–2460.

[45] Liu, M.; Li, Y.; Chen, P.; Sun, J.; Ma, D.; Li, Q.; Gao, T.; Gao, Y.; Cheng, Z.; Qiu, X.; Fang, Y.; Zhang, Y.; Liu, Z. Quasi-Freestanding Monolayer Heterostructure of Graphene and Hexagonal Boron Nitride on Ir(111) with a Zigzag Boundary. *Nano Lett.* **2014**, *14*, 6342–6347.

[46] Hwang, B.; Hwang, J.; Yoon, J. K.; Lim, S.; Kim, S.; Lee, M.; Kwon, J. H.; Baek, H.; Sung, D.; Kim, G.; Hong, S.; Ihm, J.; Stroscio, J. A.; Kuk, Y. Energy Bandgap and Edge States in an Epitaxially Grown Graphene/h-BN Heterostructure. *Sci. Rep.* **2016**, *6*, 31160.

[47] Gao, Y.; Zhang, Y.; Chen, P.; Li, Y.; Liu, M.; Gao, T.; Ma, D.; Chen, Y.; Cheng, Z.; Qiu, X.; Duan, W.; Liu, Z. Toward Single-Layer Uniform Hexagonal Boron Nitride-Graphene Patchworks with Zigzag Linking Edges. *Nano Lett.* **2013**, *13*, 3439–3443.

[48] Li, Q.; Zou, X.; Liu, M.; Sun, J.; Gao, Y.; Qi, Y.; Zhou, X.; Yakobson, B. I.; Zhang, Y.; Liu, Z. Grain Boundary Structures and Electronic Properties of Hexagonal Boron Nitride on Cu(111). *Nano Lett.* **2015**, *15*, 5804–5810.

[49] Henck, H.; Pierucci, D.; Fugallo, G.; Avila, J.; Cassabois, G.; Dappe, Y. J.; Silly, M. G.; Chen, C.; Gil, B.; Gatti, M.; Sottile, F.; Sirotti, F.; Asensio, M. C.; Ouerghi, A. Direct Observation of the Band Structure in Bulk Hexagonal Boron Nitride. *Phys. Rev. B* **2017**, *95*, 085410.

[50] Usachov, D.; Adamchuk, V. K.; Haberer, D.; Grüneis, A.; Sachdev, H.; Preobrajenski, A. B.; Laubschat, C.; Vyalikh, D. V. Quasifreestanding Single-Layer Hexagonal Boron Nitride as a Substrate for Graphene Synthesis. *Phys. Rev. B - Condens. Matter Mater. Phys.* **2010**, *82*, 075415.

[51] Hwang, J.; Hwang, H.; Kim, M.-J.; Ryu, H.; Lee, J.-E.; Zhou, Q.; Mo, S.-K.; Lee, J.; Lanzara, A.; Hwang, C. Hole Doping, Hybridization Gaps, and Electronic Correlation in Graphene on a Platinum Substrate. *Nanoscale* **2017**, *9*, 11498.

[52] Klimovskikh, I. I.; Tsirkin, S. S.; Rybkin, A. G.; Rybkina, A. A.; Filianina, M. V.; Zhizhin, E. V.; Chulkov, E. V.; Shikin, A. M. Nontrivial Spin Structure of Graphene on Pt(111) at the Fermi Level due to Spin-Dependent Hybridization. *Phys. Rev. B.* **2014**, *90*, 235431.

[53] Klimovskikh, I. I.; Otrokov, M. M.; Voroshnin, V. Y.; Sostina, D.; Petaccia, L.; Di Santo, G.; Thakur, S.; Chulkov, E. V.; Shikin, A. M. Spin-Orbit Coupling Induced Gap in Graphene on Pt(111) with Intercalated Pb Monolayer. *ACS Nano* **2017**, *11*, 368–374.

[54] Han, N.; Liu, H.; Zhang, J.; Gao, J.; Zhao, J. Atomistic Understanding of the Lateral Growth of Graphene from the Edge of an H-BN Domain: Towards a Sharp in-Plane Junction. *Nanoscale* **2017**, *9*, 3585–3592.

[55] Cattelan, M.; Agnoli, S.; Favaro, M.; Garoli, D.; Romanato, F.; Meneghetti, M.; Barinov, A.; Dudin, P.; Granozzi, G. Microscopic View on a Chemical Vapor Deposition Route to Boron-Doped Graphene Nanostructures. *Chem. Mater.* **2013**, *25*, 1490–1495.

[56] De Souza, F. A. L.; Amorim, R. G.; Scopel, W. L.; Scheicher, R. H. Nano-Structured Interface of Graphene and H-BN for Sensing Applications. *Nanotechnology* **2016**, *27*, 365503.

[57] Petrushenko, I. K.; Petrushenko, K. B. Hydrogen Adsorption on Graphene, Hexagonal Boron Nitride, and Graphene-like Boron Nitride-Carbon Heterostructures: A Comparative Theoretical Study. *Int. J. Hydrogen Energy* **2018**, *43*, 801–808.

[58] Song, X.; Sun, J.; Qi, Y.; Gao, T.; Zhang, Y.; Liu, Z. Graphene/h-BN Heterostructures: Recent Advances in Controllable Preparation and Functional Applications. *Adv. Energy Mater.* **2016**, *6*, 1600541.

[59] Bhowmick, S.; Singh, A. K.; Yakobson, B. I. Quantum Dots and Nanoroads of Graphene Embedded in Hexagonal Boron Nitride. *J. Phys. Chem. C* **2011**, *115*, 9889–9893.

[60] Giannozzi, P.; Baroni, S.; Bonini, N.; Calandra, M.; Car, R.; Cavazzoni, C.; Ceresoli, D.; Chiarotti, G. L.; Cococcioni, M.; Dabo, I.; Dal Corso, A.; De Gironcoli, S.; Fabris, S.; Fratesi, G.; Gebauer, R.; Gerstmann, U.; Gougoussis, C.; Kokalj, A.; Lazzeri, M.; Martin-Samos, L.; Marzari, N.; Mauri, F.; Mazzarello, R.; Paolini, S.; Pasquarello, A.; Paulatto, L.; Sbraccia, C.; Scandolo, S.; Sclauzero, G.; Seitsonen, A. P.; Smogunov, A.; Umari, P.; Wentzcovitch, R. M. QUANTUM ESPRESSO: A Modular and Open-Source Software Project for Quantum Simulations of Materials. *J. Phys. Condens. Matter* **2009**, *21*, 395502.

[61] Hamada, I.; Otani, M. Comparative van Der Waals Density-Functional Study of Graphene on Metal Surfaces. *Phys. Rev. B* **2010**, *82*, 153412.

[62] Tersoff, J.; Hamann, D. R. Theory of the Scanning Tunneling Microscope. *Phys. Rev. B* **1985**, *31*, 805–813.

[63] Lee, C.; Yang, W.; Parr, R. G. Development of the Colle-Salvetti Correlation-Energy Formula into a Functional of the Electron Density. *Phys. Rev. B* **1988**, *37*, 785–789.

[64] Becke, A. D. Density - Functional Thermochemistry . III . The Role of Exact Exchange Density-Functional Thermochemistry . III . The Role of Exact Exchange. *J. Chern. Phys.* **2005**, *98*, 5648–5652.

[65] Dovesi, R.; Orlando, R.; Erba, A.; Zicovich-Wilson, C. M.; Civalleri, B.; Casassa, S.; Maschio, L.; Ferrabone, M.; De La Pierre, M.; D'Arco, P.; Noël, Y.; Causà, M.; Rérat, M.; Kirtman, B. C RYSTAL14: A Program for the Ab Initio Investigation of Crystalline Solids. *Int. J. Quantum Chem.* **2014**, *114*, 1287–1317.

[66] R. Dovesi, V. R. Saunders, C. Roetti, R. Orlando, C. M. Zicovich-Wilson, F. Pascale, B. Civalleri, K. Doll, N. M. Harrison, I. J. Bush, et al. Crystal14 User's Manual. University of Torino: Torino, Italy, **2014**.

# Electronic Supplementary Material

# Click and type your title here. The font is Minion Pro bold 18. Capitalize the initial letter of the first word only. The title must be brief and grammatically correct

Type author names here. The font is "Helvetica 10". Please spell out first names and surnames. Do not include professional or official titles or academic degrees. Place an "(✉)" by the corresponding author(s). For example, First A. Firstauthor[1,2] (✉), Second B. Secondauthor[2,†], and Third C. Thirdauthor[1] (✉)

*Type author addresses here. The font is Minion Pro 9. The affiliation should be the institution where the work was conducted. If the present address of an author differs from that at which the work was carried out, please give the present address as well. For example,*

[1] *First address, Department, University, City and Postcode, Country*

[2] *Second address, Department, University, City and Postcode, Country*

[†] *Present address: Department, University, City and Postcode, Country*

Supporting information to DOI 10.1007/s12274-****-****-* (automatically inserted by the publisher)

**INFORMATION ABOUT ELECTRONIC SUPPLEMENTARY MATERIAL**. The font is Minion Pro 9.5. Electronic supplementary material (ESM) may include large artwork, lengthy descriptions, and extensive data. Each supporting information artwork, description, and data file should be referred to in the manuscript at least once. The format is "Fig. S1 in the Electronic Supplementary Material (ESM)", or "Figure S2 in the ESM" at the beginning of a sentence. A brief description of the ESM should be included in the main text, before the references section, in a paragraph entitled "Electronic Supplementary Material:". ESM should be submitted with the manuscript and will be sent to referees during peer review. Authors should ensure that it is clearly presented.

Address correspondence to First A. Firstauthor, email1; Third C. Thirdauthor, email2